ACS APPLIED NANO MATERIALS

www.acsanm.org

Article

Luminescent CdSe Quantum Dot Arrays for Rapid Sensing of Explosive Taggants

Eduardo Aznar-Gadea, Pedro J. Rodriguez-Canto, Sandra Albert Sánchez, Juan P. Martínez-Pastor, and Rafael Abargues*

Cite This: *ACS Appl. Nano Mater.* 2022, 5, 6717−6725

Read Online

ACCESS | Metrics & More | Article Recommendations | Supporting Information

ABSTRACT: Chemical sensors based on fluorescent quantum dots have attracted intense interest because of their excellent optical and electronic properties compared to the routinely employed fluorescent organic dyes. This study reports a CdSe QD-polymer-based luminescent chemosensor, which is based on an array containing either green-emitting or red-emitting CdSe QDs embedded in polycaprolactone as a polymer host matrix. We evaluate the sensing capability of the nanocomposites by exposing both sensors to vapors of explosive taggants, explosive-like molecules, and some common solvents. Both nanocomposites exhibit a very fast response time of <30 s. The limit of detection of the sensors for 3-nitrotoluene, 4-nitrotoluene 2,3-dimethyl-2,3-dinitrobutane, and picric acid was found to be 0.055, 2.7, 0.7 and 916.4 ng, respectively. The sensor array constitutes a powerful tool to discriminate between explosive taggants (3-nitrotoluene, 4-nitrotoluene, and 2,3-dimethyl-2,3-dinitrobutane) and shows specific molecular recognition toward picric acid. This type of miniaturized luminescent QD-based nanocomposites might form the basis of a sensing platform technology to perform effective chemical detection and identification of explosive taggants preblast and postblast.

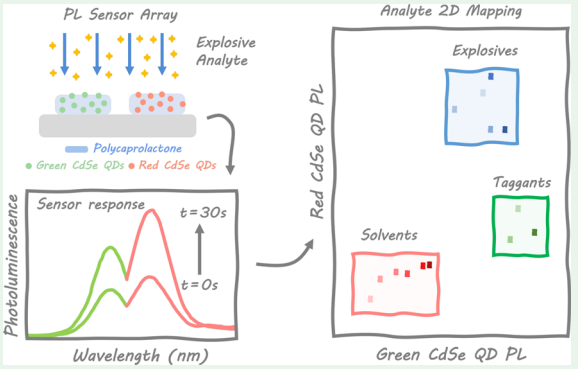

KEYWORDS: *quantum dots, sensor, multichannel, explosive taggant, 3-nitrotoluene, nanocomposite, fluorescence*

INTRODUCTION

The development of selective, sensitive, and fast detection sensors to detect explosives and explosive-like molecules is necessary to safeguard in areas such as public security, environmental safety, human health, forensic research, and anti-terrorism operations.[1,2] However, the vapor-phase detection of nitro explosives such as picric acid (PA) and 2,4,6-trinitrotoluene (TNT) is challenging because most of them have an extremely low vapor pressure at ambient temperature (PA = 5.8 × 10^{-9} mmHg; TNT = 5.50 × 10^{-6} mmHg at 25 °C). For that purpose, the addition of explosive taggants with a higher vapor pressure (10^{-2} to 10^{-3} mmHg at 25 °C) is mandatory to improve the detection of all manufactured explosives.[3] For instance, the three isomers of nitrotoluene are used as taggants for TNT,[4,5] whereas 2,3-dimethyl-2,3-dinitrotoluene is used as a taggant in plastic explosives such as C-4 (91% RDX) and Semtex (40−76% PETN).[6−8]

Trained dogs[9] and several instrumental techniques such as gas chromatography−ion mobility spectrometry,[10] surface-enhanced Raman spectroscopy,[11] gas chromatography−mass spectrometry,[12] X-ray diffraction,[13] and electrochemical methods[14] have been employed to detect and quantify explosives. Although these analytical methods show good selectivity and sensitivity, most of them have many drawbacks such as time-consuming processes and expensive, complex, and cumbersome instrumentation, which limit on-field sampling.[15,16]

Good selectivity, sensitivity, and short response time combined with profitability, robustness, and portability enabling easier use in the field are the desirable properties that an explosive sensor should have.[17] In the last few years, chemical sensors based on optical transduction mechanisms such as absorbance and fluorescence have been used to detect explosives due to their ease of incorporation in portable devices and high sensitivity.[18] Recently, we reported two molecularly imprinted polymer (MIP) nanocomposites to identify and quantify trace amounts of explosive taggants in the vapor phase. One sensing platform was based on Ag nanoparticles (NPs) embedded in the PEI as a polymer matrix and 3-nitrotoluene (3-NT) as a template to generate specific molecular recognition sites for detecting and

Received: February 17, 2022
Accepted: April 27, 2022
Published: May 11, 2022

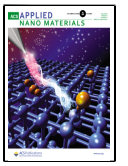

quantifying 3-NT vapors. As a result, the sensor combined the localized surface plasmon resonance of the Ag NPs with the high selectivity of the MIP. Although the chemosensor exhibited a low limit of detection (LOD) and high selectivity, the response time of the sensing platform was too slow. Consequently, their application would be limited to specific fields, such as sentinels in cargo ship containers.[19] The other gas sensor system consisted of two fluorescent molecularly imprinted nanocomposites based on $CsPbBr_3$ nanocrystals embedded in polycaprolactone (PCL) as a host matrix using 3-NT and nitromethane (NM) as template molecules for sensing and quantifying trace amounts of 3-NT. These sensors combined the optical properties of the $CsPbBr_3$ nanocrystals and the high selectivity provided by the MIP to show a strong and very fast response after exposure with a low LOD.[20] Other fluorescent materials including conjugated polymers,[16] metal−organic frameworks,[21] quantum dots (QDs),[22] nanofibrous materials,[23] MIP nanocomposites,[24] hybrid perovskites,[25] among others,[26] were also employed to detect trace amounts of explosives or explosive taggants due to their advantages such as short response time, real-time response, low LOD, and high selectivity.[27]

Explosive sensors based on QDs have been studied because of their excellent properties such as the high photoluminescence quantum yield, easiness in surface functionalization with different ligands, size-tunable emission, and good solution processability and photostability.[28,29] Moreover, these materials can be used in other applications such as photodetectors,[30−32] light-emitting diodes,[33] photocatalysts,[34] and solar energy converters.[35] In order to increase the mechanical properties and the stability of the solid-state QD sensors, the QDs can be embedded in a polymer matrix and their properties combined to achieve multifunctional materials.[36−38] Moreover, the possibility of QD functionalization with the desired ligands helps to obtain a homogeneous dispersion inside the polymer and makes them an excellent active material to build a sensing platform. The transduction mechanism of the sensor is based on changes in the QD emission when analytes interact with the QD surface. Because the PL of QDs is very sensitive to any change in their surroundings, eventual chemical or physical interactions between the analyte and the QD surface may result in noticeable changes in the PL parameters such as the peak wavelength, intensity, and bandwidth.[39] For that reason, QD nanocomposites have been reported to sense humidity,[40] temperature,[41] metal ions,[42] amines,[43] thiols,[43] and nitro compounds,[44,45] providing fast response time and high selectivity and sensitivity. Depending on the functionalization of the surface of the QDs, the sensor's sensitivity can also be improved.[46] For instance, Freeman and Willner[47] synthesized NADH-capped CdSe/ZnS QDs to detect 1,3,5-trinitrotriazine (RDX) in solution with a LOD of 0.1 nM. The authors reported that the Zn^{2+} ions of the QD shell could activate the reduction of the RDX by NADH and transform it into the non-fluorescent NAD^+-CdSe/ZnS form. Komikawa et al.[48] reported the application of peptide-modified CdTe/CdS QDs in an aqueous solution for TNT detection with high sensitivity and selectivity; after a few seconds, the fluorescence quenching can be observed by the naked eye. As can be observed, due to the low volatility of the explosives, most of the research in the state-of-the-art literature was based on solution detection.

Nevertheless, detecting explosives and explosive-like molecules directly on-field is vital to developing optical sensors for vapor phase sensing. Wu et al.[49] fabricated a sensor array of ZnS QD loaded in nanofibrous membranes to detect nitroaromatic explosive vapors. The sensing platform was synthesized by changing the ligands on the ZnS QD surface to detect and distinguish between four different explosives after 2 min of exposure. QDs sensing processes are mainly based on photo-induced electron transfer or fluorescence resonance energy transfer mechanisms between the QD and the analyte, causing fluorescence quenching.[27,39]

The application of QD sensor arrays for explosive sensing can enhance the sensitivity and also the selectivity of the sensors due to the combination of multiple outputs, which is possible because of the narrow size-tunable light emission of the QDs.[50−52] Peveler et al.[53] reported a sensor array based on CdSe QDs with different surface ligands to detect and discriminate five types of explosives in solution with a LOD lower than 0.2 ppm. The different interactions between the ligands and the analytes produced a fluorescent fingerprint for each analyte, providing both high sensitivity and selectivity. Bright et al.[54] developed a sensor array based on a nanocomposite of CdSe QDs and five organic polymers to identify some analytes in the vapor phase. The sensing platform was exposed to the vapors of two series, one of 14 different substituted benzene compounds and the other with 14 analytes related to security concerns. Linear discriminate analysis was used to distinguish the different analytes with more than 93% accuracy. Although most of the explosive sensors reported to date show good sensitivity and selectivity, the identification and quantification of trace amounts of explosives in the vapor phase are still challenging.

In this study, we report a cross-reactive heterogeneous sensing array consisting of two nanocomposites, which are formulated with CdSe QDs emitting at 560 nm (green QDs) and 597 nm (red QDs) embedded in PCL as a host polymer matrix. The sensing system was evaluated for the fast detection and analyte discrimination capability when exposed to different explosive taggants and other nitro-containing compounds in the vapor phase. The transduction mechanism of the sensor is based on changes in the PL intensity when molecules are adsorbed on the QD surface. We found that the green and red QD nanocomposite sensor array shows a different response when exposed to different analytes. Therefore, it is possible to build up reliable fingerprints in a two-dimensional (2D) map, which enables the detection and identification of the analyte while maintaining low false alarm rates. Different cycles of 3-NT/bake determined the partial reversibility of the sensing process in both CdSe QDs. These facts confirm the weak interaction between the analyte and the surface of the QDs. The green CdSe−PCL nanocomposite showed a LOD of 54.8 pg, equivalent to 1.37 ppt or 10 pM.

EXPERIMENTAL SECTION

Reagents and Materials. PCL (average molecular weight: 80,000, pellets), cadmium oxide powder, oleic acid (OA), selenium powder, trioctylphosphine (TOP), 2-mercaptoethanol (2-MET, 98%), ethylenediamine (EDA, 99%), 3-NT (99%), PA (98%, moistened with water), 1-nitronaphthalene (1-NN, 98%), and 2,3-dimethyl-2,3-dinitrobutane (DMDNB, 98%) were purchased from Sigma-Aldrich. 1-Octadecene (ODE, 90%) was purchased from Merck. *O*-xylene, toluene, acetonitrile (ACN), acetone, hexane, and methanol (MeOH) were purchased from Fisher Chemical. 4-Nitrotoluene (4-NT, 99%), 5-nitroisoquinoline (5-NI, 98%), NM (99+ %), and 4-nitrophenol (4-NP, 99%) were purchased from Acros Organics.

https://doi.org/10.1021/acsanm.2c00743
ACS Appl. Nano Mater. 2022, 5, 6717−6725

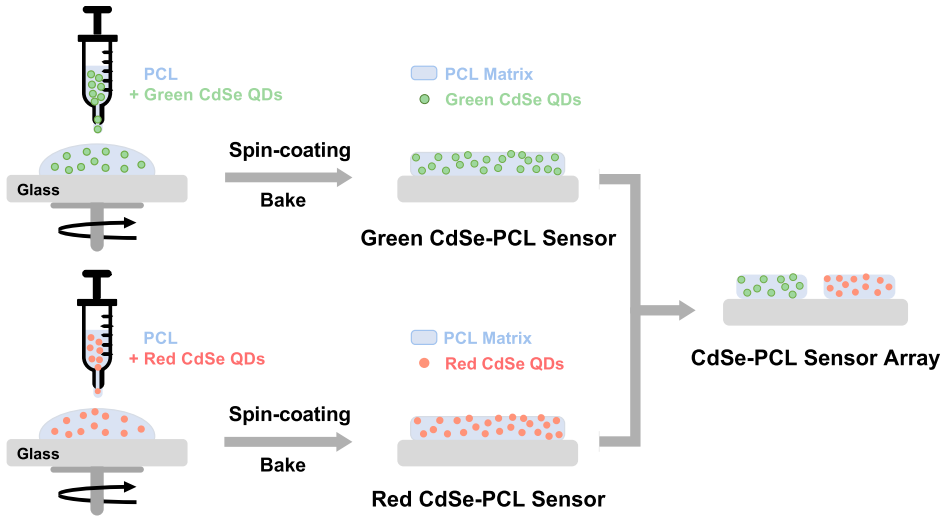

Figure 1. Schematic approach to synthesize the CdSe−PCL sensor array.

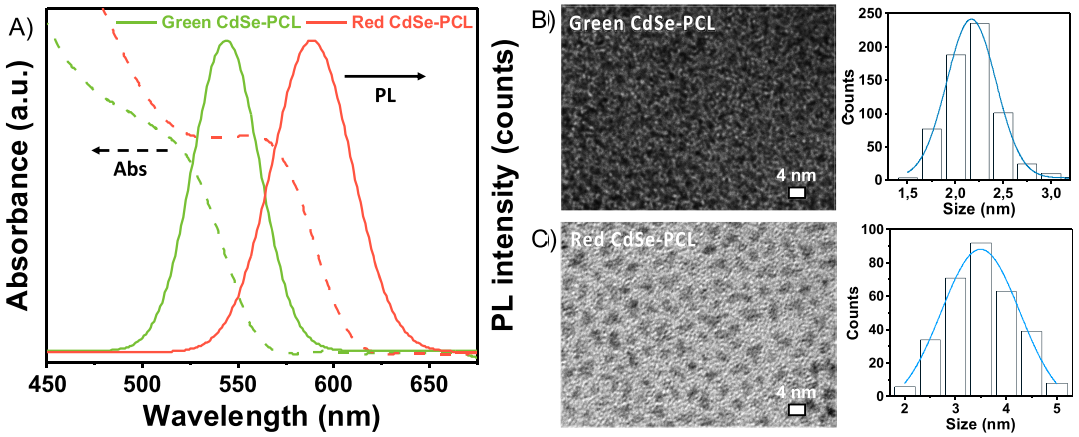

Figure 2. (A) UV−visible absorption and emission spectra of both green and red CdSe QD−PCL thin films. (B) TEM image and size distribution of green CdSe QD−PCL (C). TEM image and size distribution of red CdSe QD−PCL.

Synthesis and Purification of CdSe QDs. CdSe QDs were synthesized by a conventional synthesis route based on a hot injection method with some modifications.[55] In brief, a mixture of CdO (9 mmol), OA (54 mmol), and ODE was loaded in a 100 mL three-neck flask and heated under vacuum at 120 °C for 30 min. Consequently, this mixture was heated up to 230 °C for the complete dissolution of precursors under an N_2 atmosphere. After that, a mixture of Se (6 mmol) and TOP (29.8 mmol) was heated to obtain a transparent solution and then it was swiftly injected into the CdO solution. In order to obtain the green-emitting CdSe QDs, the reaction system was cooled, and, after 30 s, 10 mL of ODE was injected. The procedure to obtain the red-emitting QDs is similar, but after the injection the mixture was reacted for 5 min for the growth of the QDs. Both the obtained CdSe QDs were purified by several successive precipitation and redispersion steps with a mixture of acetone and methanol and redispersed in *o*-xylene with a final concentration of 20 mg/mL.

CdSe−PCL Nanocomposite Preparation and Device Fabrication. Solutions of CdSe QDs and PCL were prepared in *o*-xylene. The solution was mixed under stirring for 15 min to obtain a homogeneous dispersion. The final CdSe−PCL solution consists of 8.0 wt % PCL and 0.4612 mg/mL green-emitting CdSe QDs or 0.1678 mg/mL red-emitting CdSe QDs. The sensor was fabricated by spin-coating the CdSe−PCL solutions on a 0.5 cm^2 glass slide substrate at 2000 rpm for 30 s. Afterward, the sensors were baked at 100 °C for 10 min to remove the solvent, achieve good adhesion of the nanocomposite to the substrate, and enhance the chemical stability of the layer. Both sensors were glued on a 2 × 2 cm glass slide substrate to obtain a multichannel array. Sensors with green and red QDs were chosen to avoid the overlapping of their PL spectra, which allows the measurement of the response of both sensors simultaneously. The film thickness of the resulting sensors was measured to be around 750 nm using a mechanical profilometer (Veeco Dektack 150).

Characterization Techniques. Optical absorbance spectra of the colloidal solution containing CdSe QDs in *o*-xylene and CdSe QDs embedded in the PCL host matrix were measured at room temperature using a UV−visible spectrophotometer (PerkinElmer lambda 20 UV−vis spectrophotometer). The photoluminescence spectra of the nanocomposite thin films containing CdSe QDs were obtained upon the sensors' excitation with a CW GaN laser (404 nm) for green- and red-emitting nanocomposites. The PL quantum yield was determined to be 30% for both green and red CdSe QDs using an integrated sphere (Hamamatsu model C9920-0). Transmission electron microscopy (TEM) was carried out at an accelerating voltage of 100 kV using a JEOL 1010 microscope.

Sensing Protocol. The sensing capability of the CdSe−PCL sensors was tested by exposing the nanocomposites to the vapors of 0.2 g of different nitro compounds and common solvents in a closed 100 mL vessel at room temperature for different times (Figure S1A). The calibration curve was obtained by exposing the green CdSe sensor to the vapors of 40 mL aqueous solution using different concentrations of the analyte. The PL sensitivity and response time of the nanocomposites were measured by a homemade setup (Figure

https://doi.org/10.1021/acsanm.2c00743
ACS Appl. Nano Mater. 2022, 5, 6717−6725

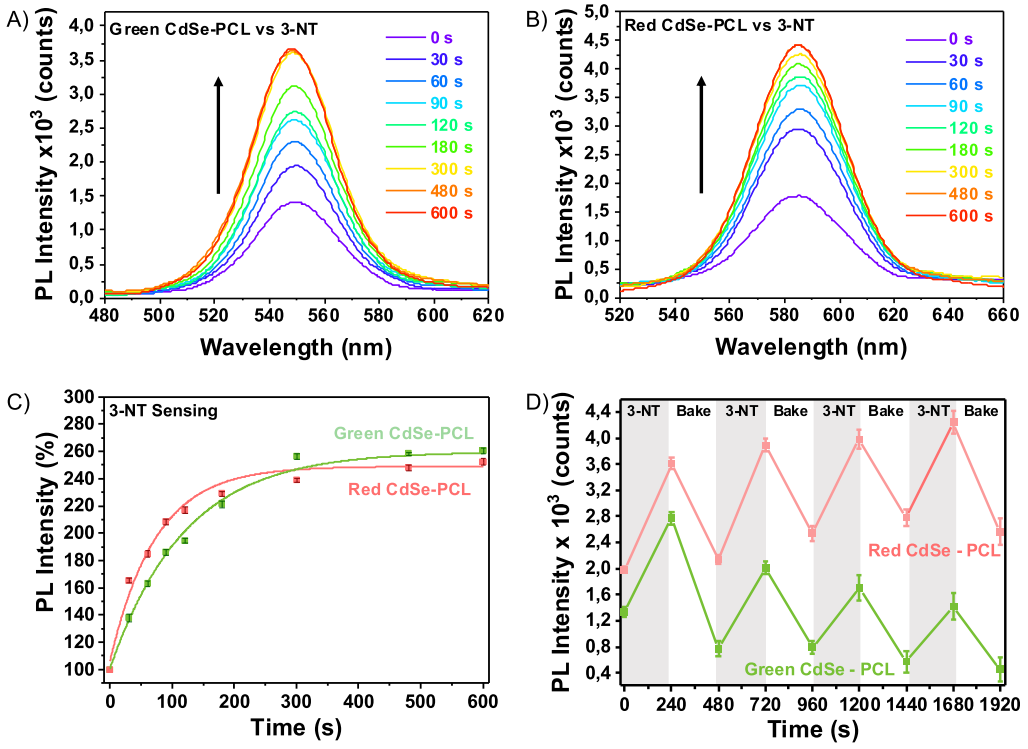

Figure 3. Fluorescence spectrum changes of the CdSe–PCL sensor array containing (A) green CdSe QDs and (B) red CdSe QDs upon exposure to 3-NT. (C) Real-time response of the two-segmented sensor upon exposure to 3-NT vapors. (D) Real-time response of green and red CdSe–PCL sensors to periodic cycles of 3-NT vapors (gray area) and mild thermal annealing at 100 °C (white area).

S1B) based on a CW GaN laser (404 nm) focused onto the sensor using a lens and positioning system to obtain precise and reproducible results and a commercial spectrophotometric system NanoSPR103 (NANOSPR). The sensing and detection conditions were performed in the dark in order to obtain good PL measurements. Moreover, all experiments were performed three times to evaluate the stability of the sensors and the reproducibility of the data, and good results were obtained.

RESULTS AND DISCUSSION

Synthesis and Characterization of CdSe–PCL Sensors. The synthesis of the CdSe–PCL sensors was straightforward and consisted of a single step, as is illustrated in Figure 1. First, a solution of PCL and green or red CdSe QDs in *o*-xylene was spin-coated on a glass substrate and baked at 100 °C to remove the solvent. The sensor array consisted of two different nanocomposite films formulated with green and red CdSe QDs embedded in PCL. This system was designed to detect and discriminate a range of explosives and explosives-like molecules. PCL is a biodegradable, hydrophobic, and inexpensive polymer with a low melting point (59–64 °C) and glass-transition temperature (−60 °C) and is considered an excellent host matrix for CdSe QDs because it shows exceptional film-forming properties and outstanding blend compatibility with oleate-capped CdSe QDs.[16,56,57]

Figure 2A shows the absorbance and PL spectra of the green and red CdSe QD–PCL thin film. The first energy exciton state of the CdSe–PCL nanocomposites was observed at 515 nm for green-emitting QDs and at 558 nm for red-emitting QDs. The emission peak of the green and red CdSe QDs embedded in the PCL was located at 543 nm (fwhm: 40 nm) and 588 nm (fwhm: 49 nm), respectively. The absorbance and PL of the nanocomposite thin films show a blue shift with respect to the green and red CdSe QD solution in *o*-xylene (see Figure S2A,B in the Supporting Information). Mainly, PL shows a significant blue shift from 560 and 596 nm to 543 and 588 nm when the green and red QDs are embedded in the polymer. Figure 2B,C shows TEM images of the green and red CdSe QDs and their corresponding size distribution. We calculated an average size of 2.2 ± 0.5 nm for green CdSe–PCL and of 3.6 ± 0.7 nm for red CdSe–PCL. The average size of colloidal green and red CdSe QDs was 2.4 ± 0.3 and 3.6 ± 0.8 nm, respectively (see Figures S3,S4 in the Supporting Information). These results confirm that the size distribution of the green and red CdSe QDs remains constant after the formation of the nanocomposite. The PL blue shift after the formation of the nanocomposite may be mainly attributed to a decrease of the effective refractive index surrounding the QDs caused by the porosity of the polymer matrix. Scanning electron microscopy (SEM) images of both nanocomposites reveal a homogeneous, flat, and smooth surface (see Figure S5 in the Supporting Information).

Analyte Sensing. The evaluation of the sensing capability of the nanocomposites was performed by exposing the sensor array to 3-NT vapors in a 100 mL closed vessel at room temperature. The concentration of 3-NT in the vapor phase depends on the vapor pressure of the analyte because the mass transport is caused by a diffusion process. Figure 3 exhibits the PL response of the green CdSe–PCL (Figure 3A) and red CdSe–PCL (Figure 3B) nanocomposites upon exposure to vapors of 3-NT for different times. The measurements were done, providing enough time to interact the analyte with the sensor. The exposure of the sensor array to 3-NT led to significant PL enhancement. Remarkably, the change in the PL intensity is quite different depending on the nanocomposite. As can be observed, the exposure of the sensor array to 3-NT led to significant PL enhancement within the first 30 s in both

https://doi.org/10.1021/acsanm.2c00743
ACS Appl. Nano Mater. 2022, 5, 6717–6725

nanocomposites (138.2% green CdSe−PCL and 165.6% red CdSe−PCL). Wu et al.[49] reported a time response of 2 min for ZnS QDs for nitroaromatic compounds, whereas Bright et al.[54] reported 60 s for the CdSe QD nanocomposite array.

The time-dependent PL changes of the sensor array containing green and red QDs to 3-NT vapors is plotted as a function of exposure time using PL intensity as a response variable (Figure 3C). The experimental data obtained for the 3-NT exposure can be fitted by the following pseudo-first-order kinetic equation proposed by Lagergren, which describes the diffusion of the analytes:[19,43,58] $PL_t = PL_\infty + Ae^{-k \cdot t}$, where PL_t is the PL intensity at a given time, PL_∞ is the response when the sensor is saturated by the analyte, and k is the binding rate constant. The results obtained from fitting the real-time PL response are listed in Table 1.

Table 1. Maximum PL Intensity and Kinetic Binding Constant for the CdSe−PCL Sensor Array Exposed to 3-NT Vapors

sensor	PL_∞ (%)	k (ms−1)
green CdSe−PCL	260 ± 3	8.35 ± 0.11
red CdSe−PCL	249 ± 4	13.61 ± 0.13

As can be observed, the interaction between the analyte molecules and the CdSe QDs embedded in the PCL matrix depends on the time exposure, which is determined by the diffusion of the analyte and the subsequent chemical interaction rate.[43,59] The kinetic constant depends on the amount of available CdSe QDs (binding sites) embedded in the polymer matrix and also on the mass concentration of analyte in the vapor phase, which is directly related to the vapor pressure of the analyte. For that reason, the maximum binding rate is achieved at the beginning of the sensing process, when almost all of the binding sites are unoccupied. As a result, the limiting step changes during the sensing process. While the mass transport from the vapor phase to the QD surface principally controlled the first stages of the sensing test, the interaction between the analyte and CdSe QDs limited the later steps. Red CdSe QD−PCL shows a faster analyte binding kinetics (k = 13.61 ms^{-1}) than that of green QD−PCL (k = 8.35 ms^{-1}). The differences are more significant at low sensing times. After 30 s, green and red CdSe QD−PCL exhibits PL enhancements of 138.2 and 165.6%, respectively. However, after 180 s of exposure to 3-NT vapors, both sensors show more than 220% PL enhancement. Both sensors shows similar PL_∞.

The mechanism of PL enhancement is not fully understood, but some mechanisms are stated in the literature. The increase of fluorescence can be explained by a hybrid steric/electronic mechanism. The change in the PL intensity might be due to the disruption of the steady-state complex formed by CdSe QDs and PCL in the nanocomposite. The polymer matrix probably creates trap states on the QD surface that affect the QD fluorescence properties. When the vapor analytes diffuse within the matrix, they can cause the polymer to swell. As a

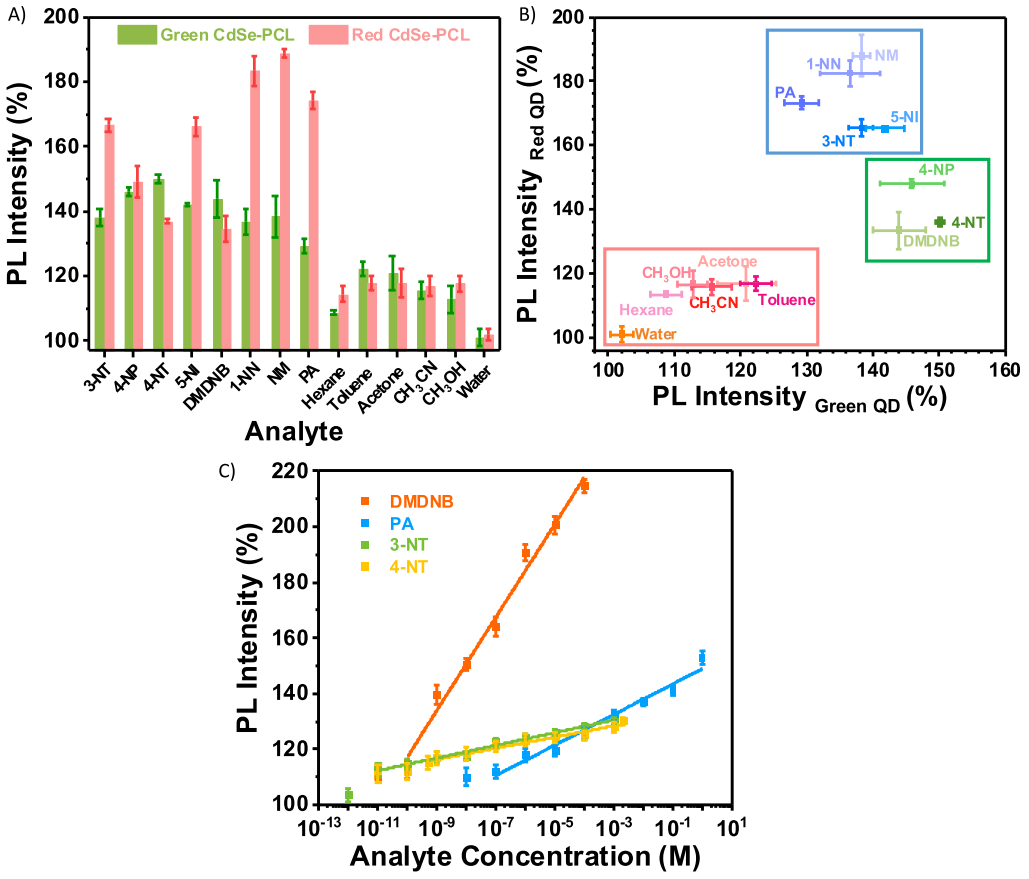

Figure 4. (A) Selectivity of the CdSe−PCL sensor array to different NO_2-containing compounds and some common solvents after 30 s of exposure. (B) 2D map of the PL efficiency of both nanocomposites after 30 s of exposure. () Calibration curve of the green CdSe−PCL sensor. PL enhancement as a function of 3-NT, 4-NT, DMDNB, and PA concentrations after 20 min of exposure.

https://doi.org/10.1021/acsanm.2c00743
ACS Appl. Nano Mater. 2022, 5, 6717−6725

result, the steady-state complex can be interrupted by the detachment of the polymer chains from the CdSe QD surface, leading to a change in the fluorescence properties.[54,60] Therefore, the observed PL enhancement can mainly be ascribed to the swelling induced in the polymer when exposed to volatile organic compound analytes. Moreover, once the PCL chains separate from the QD surface, the analyte can interact directly with the QD surface. Analytes can act as pseudoligands to passivate trap states with different effectiveness depending on their composition. This affect the PL properties of QDs accordingly, as shown by other ligand exchange studies.[30,34] Interestingly, PL enhancement when exposed to 3-NT is generally faster in red CdSe−PCL than in green CdSe PCL. The swelling rate of CdSe−PCL is probably dependent on the QD size. The size of the QDs can be affected by the swelling because the spacing between the polymer chains increases with the size of the QDs. Because the green QDs are smaller (2.2 nm) than red QDs (3.6 nm), the steady-state complex between the polymer matrix and green QDs is stronger because more intermolecular bonds are formed. It is well accepted that properties of nanocomposite are strongly affected by the nanoparticle size. Several works have reported that the nanoparticle size clearly affects various material mechanical properties such as Young's modulus,[61] the thermal expansion coefficient, the thermal conductivity, and the electrical conductivity. Therefore, one could expect that as the QD size decreases, the steady-state complex between CdSe QDs and PCL is stronger.

We also evaluated the influence of the film thickness on the sensing response. As can be observed in Figure S6 in the Supporting Information, the 380 and 750 nm-thick sensors show comparable response to 3-NT. These results suggest that the polymer matrix allows complete diffusion of the nitro-containing analytes in the film at these two film thicknesses.

Figure 3D shows the sensor reversibility. Every sensing cycle involves the exposure to 3-NT flow for 240 s, followed by a recovering cycle by baking at 100 °C for 240 s. The PL intensity increases when the nanocomposites are exposed to 3-NT vapors. After the baking step, the green CdSe−PCL sensors recover around 75% of the initial PL, but the red CdSe−PCL sensors improve the initial PL around 110%. Because most of the 3-NT molecules are weakly adsorbed on the surface of the sensors, they can be easily desorbed after mild thermal annealing. However, both sensors show certain hysteresis after every sensing/recovering cycle but with different behaviors. Whereas the green CdSe−PCL sensor exhibits a gradual PL loss after every sensing/recovering cycle, the red CdSe−PCL sensor shows a constant PL increase. In the case of green CdSe−PCL, the loss of PL is attributed to the degradation of the CdSe QD after baking. In fact, for every sensing/recovering cycle, the ratio of PL before and after sensing decays. This is expected because small QDs are thermodynamically more unstable. On the other hand, the increase of PL in the red CdSe−PCL sensor is ascribed to the non-complete removal of the analyte after baking. With every sensing/recovering cycle, more number of analyte molecules are attached to the QD surface and the PL increases. In fact, the red CdSe−PCL sensor shows a constant ratio of PL before and after sensing. This confirms that the red CdSe−PCL sensor is reversible unlike that of the green CdSe−PCL sensor.

Figure 4A shows the PL of the CdSe−PCL sensor array after 30 s of exposure to vapors of some explosive taggants (3-NT, 4-NT, and DMDNB), other NO_2-containing compounds (4-NP, 5-NI, 1-NN, NM, and PA) and some solvents (hexane, toluene, acetone, ACN (CH_3CN), methanol (CH_3OH), and water). The response of both sensors toward explosive taggants and nitro-containing molecules were higher than toward the common solvents (see Figure S7 for the green CdSe−PCL sensor and Figure S8 for the red CdSe−PCL sensor in the Supporting Information). These results indicate that the sensor array interacts more selectively with nitro-containing molecules. Because the sensor array is label-free, it does not provide highly specific sensing but selective sensing to a certain degree. The interaction between the analytes and the QD surface depends on the chemical structure of analytes. In addition, the PCL matrix provides certain degree of selectivity because it does not allow the diffusion of all analytes in the same way. This means that PCL shows specific permeability to nitro compounds, as already observed in our previous work.[20] More interestingly, both sensors show a different response to nitro-containing analytes. Specifically, the red CdSe−PCL sensor exhibited an extraordinary response to NM (188.0% PL), 1-NN (182.5% PL), and PA (173.2% PL), whereas the green CdSe−PCL sensor showed high affinity to 4-NT (150.2% PL) and DMDNB (144.0% PL). This makes it an extraordinary tool to fingerprint analytes.

When the sensor array is exposed to well-known ligand molecules like thiols (2-MET) or diamines (EDA) (see Figure S9A,B in the Supporting Information), a very fast chemical interaction between 2-MET or EDA and the CdSe QD surface is observed due to their strong affinity to transition metals like Cd(II).[43] As a result, the red and green CdSe−PCL PL decays abruptly and irreversibly.

On the basis of different responses of the green and red CdSe−PCL sensor to the analytes, the sensor array was examined for their ability to fingerprint analytes by multi-parameter analysis. Monitoring the changes in the PL of the green and red CdSe−PCL sensor array allowed us to pinpoint each analyte on a 2D map. To generate such response patterns, the PL response of green and red CdSe−PCL nanocomposites were plotted after 30 s exposure to analytes in Figure 4B. By using these two parameters, we classified the analytes into three different groups. The first group consisted of common solvents with the lowest response (low affinity for both nanocomposites). The second group was formed by those analytes with the greatest interaction with the green CdSe−PCL sensor (DMDNB, 4-NT, and 4-NP). The third group was composed of analytes which showed the highest response to the red CdSe−PCL sensor (NM, 1-NN, PA, 3-NT, and 5-NI). These results demonstrate that we can discriminate between the explosive taggants 3-NT, 4-NT, and DMDNB. Moreover, the sensor array showed specific molecular recognition toward PA, an explosive of great importance. Wu et al.[49] and Peveler et al.[53] described a sensing platform with which one can distinguish between four and five explosive compounds, respectively.

Figure 4C presents the green CdSe−PCL sensor response to vapors of different concentrations of 3-NT, 4-NT, DMDNB, and PA in water after a constant exposure time of 20 min. We focused on PA (explosive compound) and on 3-NT, 4-NT, and DMDNB (explosive taggants). From the calibration curves, we determined the LOD to quantify the minimum analyte amount that the sensor would be able to detect. We also calculated the sensor sensitivity, which is defined as the sensor response per logarithmic unit of analyte concentration. The response of the green CdSe−PCL nanocomposite to

https://doi.org/10.1021/acsanm.2c00743
ACS Appl. Nano Mater. 2022, 5, 6717−6725

water vapors showed a PL increase of only 10% after 20 min (see Figure S10 in the Supporting Information), which was considered as the blank from which the detection is feasible. The assumption is that if an analyte is present, the sensor will produce a response greater than the analytical noise in the absence of an analyte. The experimental LOD, sensor sensitivity, and linear range are listed in Table 2.

Table 2. LOD, Sensitivity, and Linear Range for the Green CdSe−PCL Sensor Exposed to Different Analyte Vapors

analyte	LOD (ppb)	sensitivity (% PL)	linear range (M)
3-NT	0.0014	2.28 ± 0.11	10^{-11} to 10^{-3}
4-NT	0.068	2.01 ± 0.12	5×10^{-10} to 10^{-3}
DMDNB	0.088	16.76 ± 0.91	10^{-10} to 10^{-4}
PA	22.9	5.50 ± 0.37	10^{-7} to 1

The sensor showed the lowest LOD for 3-NT, which was determined to be 0.055 ng, equivalent to1.37 ppt or 10 pM. Generally, the green CdSe−PCL sensor showed an excellent linear response within a wide range of concentrations. For example, the sensor response to 3-NT was linear from 10^{-11} to 10^{-3} M, that is, 8 orders of magnitude. A wide-range linear response is desirable to develop a quantitative sensor. The sensor sensitivity is another important parameter, which can be determined from the slope of the linear regression of the calibration curve. The sensor had the highest sensitivity for DMDND, which is 16.76% PL per logarithmic unit of analyte concentration. The sensitivity reported by Wu et al.[49] and Peveler et al.[53] was 4 ppb and lower than 0.2 ppm, respectively.

CONCLUSIONS

The majority of the current detection methodologies focus on the fluorescence intensity change (quenching/enhancing) of a single transducer, which may be efficient in identifying analytes from different categories but will be unable to distinguish analytes having similar properties. To overcome this limitation, we reported a sensor array based on green- or red-emitting CdSe QDs embedded in PCL as a host matrix, allowing the identification and quantification of trace amounts of explosive taggants and explosive-like molecules. The experimental LOD of the green CdSe−PCL for 3-NT, 4-NT, DMDNB, and PA was found to be 0.055, 2.7, 0.7, and 916.4 ng, respectively. This sensor response was very fast and showed a very wide linear response to explosive taggants (up to 8 orders of magnitude), which forms the basis to be used as a quantitative sensor. Combining two transducers constitutes a powerful tool to discriminate between some of the most commonly used explosive taggants 3-NT, 4-NT, and DMDNB. Moreover, the sensor array showed specific molecular recognition toward PA, an explosive of great importance. Multiparametric analysis allowed us to improve the sensitivity and selectivity significantly and to minimize false-positive responses. This type of miniaturized luminescent QD-based nanocomposites might form the basis of a sensing platform technology to perform effective chemical detection and identification of explosive taggants preblast and postblast.

ASSOCIATED CONTENT

Supporting Information

The Supporting Information is available free of charge at https://pubs.acs.org/doi/10.1021/acsanm.2c00743.

Schematic picture of the sensing system and the homemade experimental setup; UV−vis absorption and emission spectra of CdSe QD in *o*-xylene and embedded in PCL; TEM images of colloidal CdSe QDs; SEM images of CdSe−PCL films; PL response of different thickness sensing platforms to 3-NT vapors; PL response of the sensor array to vapors of different nitro compounds; PL response of the two-segmented to vapors of 2-MET and EDA; and response of the green CdSe−PCL sensor to water vapors (PDF)

AUTHOR INFORMATION

Corresponding Author

Rafael Abargues − *Instituto de Ciencia de los Materiales, Universidad de Valencia, Paterna 46980, Spain;* orcid.org/0000-0001-5055-6339; Email: Rafael.Abargues@uv.es

Authors

Eduardo Aznar-Gadea − *Instituto de Ciencia de los Materiales, Universidad de Valencia, Paterna 46980, Spain;* orcid.org/0000-0002-2261-3591

Pedro J. Rodriguez-Canto − *Intenanomat S.L., Paterna 46980, Spain*

Sandra Albert Sánchez − *Intenanomat S.L., Paterna 46980, Spain*

Juan P. Martínez-Pastor − *Instituto de Ciencia de los Materiales, Universidad de Valencia, Paterna 46980, Spain;* orcid.org/0000-0003-3683-0578

Complete contact information is available at: https://pubs.acs.org/10.1021/acsanm.2c00743

Notes

The authors declare no competing financial interest.

ACKNOWLEDGMENTS

This work was supported through the NATO Science for Peace and Security Programme Project SPS (no. G5361). We acknowledge the support of the Spanish MICINN through projects Retos-Colaboración 2016 Project Safetag (no. RTC-2016-5197-2) and Retos de la Sociedad Project Nirvana (no. PID2020-119628RB-C31) by MCIN/AEI/10.13039/501100011033. R.A. acknowledges the "Agencia Valenciana de la Innovació" for the Valorizació 2018 Project Hidronio (no. INNVAL10/18/032) and the Valorizació 2021 Project CATIOX (no. INNVA1/2021/56). R. A. also thanks the Spanish MICINN for their Ramón y Cajal Fellowship (no. RYC-2015-18349). We would like to thank Dr Chegel and Dr Lopatynskyi for the fruitful discussions on sensors and explosives.

REFERENCES

(1) Long, Y.; Chen, H.; Wang, H.; Peng, Z.; Yang, Y.; Zhang, G.; Li, N.; Liu, F.; Pei, J. Highly Sensitive Detection of Nitroaromatic Explosives Using an Electrospun Nanofibrous Sensor Based on a Novel Fluorescent Conjugated Polymer. *Anal. Chim. Acta* **2012**, *744*, 82−91.

(2) Hu, T.; Sang, W.; Chen, K.; Gu, H.; Ni, Z.; Liu, S. Simple and Sensitive Colorimetric Detection of a Trace Amount of 2,4,6-Trinitrotoluene (TNT) with QD Multilayer-Modified Microchannel Assays. *Mater. Chem. Front.* **2019**, *3*, 193−198.

(3) Sun, X.; Wang, Y.; Lei, Y. Fluorescence Based Explosive Detection: From Mechanisms to Sensory Materials. *Chem. Soc. Rev.* **2015**, *44*, 8019−8061.
(4) Roucou, A.; Kleiner, I.; Goubet, M.; Bteich, S.; Mouret, G.; Bocquet, R.; Hindle, F.; Meerts, W. L.; Cuisset, A. Towards the Detection of Explosive Taggants: Microwave and Millimetre-Wave Gas-Phase Spectroscopies of 3-Nitrotoluene. *ChemPhysChem* **2018**, *19*, 1056−1067.
(5) Štejfa, V.; Kadlecová, K.; Růžička, K.; Fulem, M. Vapor Pressure and Thermophysical Properties of Explosive Taggants. *Chem. Thermodyn. Therm. Anal.* **2021**, *3-4*, 100020.
(6) Meaney, M. S.; McGuffin, V. L. Luminescence-Based Methods for Sensing and Detection of Explosives. *Anal. Bioanal. Chem.* **2008**, *391*, 2557−2576.
(7) Loch, A. S.; Stoltzfus, D. M.; Burn, P. L.; Shaw, P. E. High-Sensitivity Poly(Dendrimer)-Based Sensors for the Detection of Explosives and Taggant Vapors. *Macromolecules* **2020**, *53*, 1652−1664.
(8) Hutchinson, K. L.; Stoltzfus, D. M.; Burn, P. L.; Shaw, P. E. Luminescent Poly(Dendrimer)s for the Detection of Explosives. *Mater. Adv.* **2020**, *1*, 837−844.
(9) Furton, K.; Myers, L. J. The Scientific Foundation and Efficacy of the Use of Canines as Chemical Detectors for Explosives. *Talanta* **2001**, *54*, 487−500.
(10) Amo-González, M.; Pérez, S.; Delgado, R.; Arranz, G.; Carnicero, I. Tandem Ion Mobility Spectrometry for the Detection of Traces of Explosives in Cargo at Concentrations of Parts Per Quadrillion. *Anal. Chem.* **2019**, *91*, 14009−14018.
(11) Byram, C.; Moram, S. S. B.; Soma, V. R. SERS Based Detection of Multiple Analytes from Dye/Explosive Mixtures Using Picosecond Laser Fabricated Gold Nanoparticles and Nanostructures. *Analyst* **2019**, *144*, 2327−2336.
(12) Galmiche, M.; Colin, A.; Clavos, M.-C.; Pallez, C.; Rosin, C.; Dauchy, X. Determination of Nitroaromatic Explosive Residues in Water by Stir Bar Sorptive Extraction-Gas Chromatography-Tandem Mass Spectrometry. *Anal. Bioanal. Chem.* **2021**, *413*, 159−169.
(13) Wells, K.; Bradley, D. A. A Review of X-Ray Explosives Detection Techniques for Checked Baggage. *Appl. Radiat. Isot.* **2012**, *70*, 1729−1746.
(14) Cetó, X.; O'Mahony, A. M.; Wang, J.; del Valle, M. Simultaneous Identification and Quantification of Nitro-Containing Explosives by Advanced Chemometric Data Treatment of Cyclic Voltammetry at Screen-Printed Electrodes. *Talanta* **2013**, *107*, 270−276.
(15) Sharma, V.; Mehata, M. S. Rapid Optical Sensor for Recognition of Explosive 2,4,6-TNP Traces in Water through Fluorescent ZnSe Quantum Dots. *Spectrochim. Acta Mol. Biomol. Spectrosc.* **2021**, *260*, 119937.
(16) Toal, S. J.; Trogler, W. C. Polymer Sensors for Nitroaromatic Explosives Detection. *J. Mater. Chem.* **2006**, *16*, 2871.
(17) Li, Z.; Askim, J. R.; Suslick, K. S. The Optoelectronic Nose: Colorimetric and Fluorometric Sensor Arrays. *Chem. Rev.* **2019**, *119*, 231−292.
(18) Salinas, Y.; Martínez-Máñez, R.; Marcos, M. D.; Sancenón, F.; Costero, A. M.; Parra, M.; Gil, S. Optical Chemosensors and Reagents to Detect Explosives. *Chem. Soc. Rev.* **2012**, *41*, 1261−1296.
(19) Aznar-Gadea, E.; Rodríguez-Canto, P. J.; Martínez-Pastor, J. P.; Lopatynskyi, A.; Chegel, V.; Abargues, R. Molecularly Imprinted Silver Nanocomposites for Explosive Taggant Sensing. *ACS Appl. Polym. Mater.* **2021**, *3*, 2960−2970.
(20) Aznar-Gadea, E.; Sanchez-Alarcon, I.; Soosaimanickam, A.; Rodriguez-Canto, P. J.; Perez-Pla, F.; Martínez-Pastor, J. P.; Abargues, R. Molecularly Imprinted Nanocomposites of CsPbBr 3 Nanocrystals: An Approach towards Fast and Selective Gas Sensing of Explosive Taggants. *J. Mater. Chem. C* **2022**, *10*, 1754.
(21) Hu, Z.; Deibert, B. J.; Li, J. Luminescent Metal-Organic Frameworks for Chemical Sensing and Explosive Detection. *Chem. Soc. Rev.* **2014**, *43*, 5815−5840.
(22) Peveler, W. J.; Jaber, S. B.; Parkin, I. P. Nanoparticles in Explosives Detection − the State-of-the-Art and Future Directions. *Forensic Sci. Med. Pathol.* **2017**, *13*, 490−494.
(23) Yang, Y.; Wang, H.; Su, K.; Long, Y.; Peng, Z.; Li, N.; Liu, F. A Facile and Sensitive Fluorescent Sensor Using Electrospun Nanofibrous Film for Nitroaromatic Explosive Detection. *J. Mater. Chem.* **2011**, *21*, 11895.
(24) Ma, Y.; Xu, S.; Wang, S.; Wang, L. Luminescent Molecularly-Imprinted Polymer Nanocomposites for Sensitive Detection. *Trac. Trends Anal. Chem.* **2015**, *67*, 209−216.
(25) Harwell, J. R.; Glackin, J. M. E.; Davis, N. J. L. K.; Gillanders, R. N.; Credgington, D.; Turnbull, G. A.; Samuel, I. D. W. Sensing of Explosive Vapor by Hybrid Perovskites: Effect of Dimensionality. *APL Mater.* **2020**, *8*, 071106.
(26) To, K. C.; Ben-Jaber, S.; Parkin, I. P. Recent Developments in the Field of Explosive Trace Detection. *ACS Nano* **2020**, *14*, 10804−10833.
(27) Ma, Y.; Wang, S.; Wang, L. Nanomaterials for Luminescence Detection of Nitroaromatic Explosives. *Trac. Trends Anal. Chem.* **2015**, *65*, 13−21.
(28) Algarra, M.; Campos, B. B.; Miranda, M. S.; da Silva, J. C. G. E. CdSe Quantum Dots Capped PAMAM Dendrimer Nanocomposites for Sensing Nitroaromatic Compounds. *Talanta* **2011**, *83*, 1335−1340.
(29) Lu, H.; Carroll, G. M.; Neale, N. R.; Beard, M. C. Infrared Quantum Dots: Progress, Challenges, and Opportunities. *ACS Nano* **2019**, *13*, 939−953.
(30) Maulu, A.; Rodríguez-Cantó, P. J.; Navarro-Arenas, J.; Abargues, R.; Sánchez-Royo, J. F.; García-Calzada, R.; Pastor, J. P. M. Strongly-Coupled PbS QD Solids by Doctor Blading for IR Photodetection. *RSC Adv.* **2016**, *6*, 80201−80212.
(31) Maulu, A.; Navarro-Arenas, J.; Rodríguez-Cantó, P.; Sánchez-Royo, J.; Abargues, R.; Suárez, I.; Martínez-Pastor, J. Charge Transport in Trap-Sensitized Infrared PbS Quantum-Dot-Based Photoconductors: Pros and Cons. *Nanomaterials* **2018**, *8*, 677.
(32) Yadav, P. V. K.; Ajitha, B.; Kumar Reddy, Y. A.; Sreedhar, A. Recent Advances in Development of Nanostructured Photodetectors from Ultraviolet to Infrared Region: A Review. *Chemosphere* **2021**, *279*, 130473.
(33) Yan, L.; Shen, X.; Zhang, Y.; Zhang, T.; Zhang, X.; Feng, Y.; Yin, J.; Zhao, J.; Yu, W. W. Near-Infrared Light Emitting Diodes Using PbSe Quantum Dots. *RSC Adv.* **2015**, *5*, 54109−54114.
(34) Abargues, R.; Navarro, J.; Rodríguez-Cantó, P. J.; Maulu, A.; Sánchez-Royo, J. F.; Martínez-Pastor, J. P. Enhancing the Photocatalytic Properties of PbS QD Solids: The Ligand Exchange Approach. *Nanoscale* **2019**, *11*, 1978−1987.
(35) Yuan, M.; Liu, M.; Sargent, E. H. Colloidal Quantum Dot Solids for Solution-Processed Solar Cells. *Nat. Energy* **2016**, *1*, 16016.
(36) Gordillo, H.; Suarez, I.; Abargues, R.; Rodriguez-Canto, P.; Almuneau, G.; Martinez-Pastor, J. P. Quantum-Dot Double Layer Polymer Waveguides by Evanescent Light Coupling. *J. Light. Technol.* **2013**, *31*, 2515−2525.
(37) Gordillo, H.; Suarez, I.; Abargues, R.; Rodriguez-Canto, P.; Martinez-Pastor, J. P. Color Tuning and White Light by Dispersing CdSe, CdTe, and CdS in PMMA Nanocomposite Waveguides. *IEEE Photonics J.* **2013**, *5*, 2201412.
(38) Suárez, I.; Larrue, A.; Rodríguez-Cantó, P. J.; Almuneau, G.; Abargues, R.; Chirvony, V. S.; Martínez-Pastor, J. P. Efficient Excitation of Photoluminescence in a Two-Dimensional Waveguide Consisting of a Quantum Dot-Polymer Sandwich-Type Structure. *Opt. Lett.* **2014**, *39*, 4962.
(39) Freeman, R.; Willner, I. Optical Molecular Sensing with Semiconductor Quantum Dots (QDs). *Chem. Soc. Rev.* **2012**, *41*, 4067−4085.
(40) Ze, L.; Yueqiu, G.; Xujun, L.; Yong, Z. MoS2-Modified ZnO Quantum Dots Nanocomposite: Synthesis and Ultrafast Humidity Response. *Appl. Surf. Sci.* **2017**, *399*, 330−336.

https://doi.org/10.1021/acsanm.2c00743
ACS Appl. Nano Mater. 2022, 5, 6717−6725

(41) Bueno, A.; Suarez, I.; Abargues, R.; Sales, S.; Pastor, J. P. M. Temperature Sensor Based on Colloidal Quantum Dots−PMMA Nanocomposite Waveguides. *IEEE Sens. J.* **2012**, *12*, 3069−3074.
(42) Paramanik, B.; Bhattacharyya, S.; Patra, A. Detection of Hg 2+ and F − Ions by Using Fluorescence Switching of Quantum Dots in an Au-Cluster-CdTe QD Nanocomposite. *Chem.—Eur. J.* **2013**, *19*, 5980−5987.
(43) Rodríguez-Cantó, P. J.; Abargues, R.; Gordillo, H.; Suárez, I.; Chirvony, V.; Albert, S.; Martínez-Pastor, J. UV-Patternable Nanocomposite Containing CdSe and PbS Quantum Dots as Miniaturized Luminescent Chemo-Sensors. *RSC Adv.* **2015**, *5*, 19874−19883.
(44) Devi, S.; Kaur, R.; Paul, A. K.; Tyagi, S. MPA-Capped CdSe QD/Mercaptoethylamine-Capped AuNP Nanocomposite-Based Sensor for Instant Detection of Trinitrotoluene. *Colloid Polym. Sci.* **2018**, *296*, 427−440.
(45) Shi, G. H.; Shang, Z. B.; Wang, Y.; Jin, W. J.; Zhang, T. C. Fluorescence Quenching of CdSe Quantum Dots by Nitroaromatic Explosives and Their Relative Compounds. *Spectrochim. Acta Mol. Biomol. Spectrosc.* **2008**, *70*, 247−252.
(46) Hines, D. A.; Kamat, P. V. Recent Advances in Quantum Dot Surface Chemistry. *ACS Appl. Mater. Interfaces* **2014**, *6*, 3041.
(47) Freeman, R.; Willner, I. NAD+/NADH-Sensitive Quantum Dots: Applications To Probe NAD + -Dependent Enzymes and To Sense the RDX Explosive. *Nano Lett.* **2009**, *9*, 322−326.
(48) Komikawa, T.; Tanaka, M.; Tamang, A.; Evans, S. D.; Critchley, K.; Okochi, M. Peptide-Functionalized Quantum Dots for Rapid Label-Free Sensing of 2,4,6-Trinitrotoluene. *Bioconjugate Chem.* **2020**, *31*, 1400−1407.
(49) Wu, Z.; Duan, H.; Li, Z.; Guo, J.; Zhong, F.; Cao, Y.; Jia, D. Multichannel Discriminative Detection of Explosive Vapors with an Array of Nanofibrous Membranes Loaded with Quantum Dots. *Sensors* **2017**, *17*, 2676.
(50) Feng, S.; Farha, F.; Li, Q.; Wan, Y.; Xu, Y.; Zhang, T.; Ning, H. Review on Smart Gas Sensing Technology. *Sensors* **2019**, *19*, 3760.
(51) Xu, Q.; Zhang, Y.; Tang, B.; Zhang, C.-y. Multicolor Quantum Dot-Based Chemical Nose for Rapid and Array-Free Differentiation of Multiple Proteins. *Anal. Chem.* **2016**, *88*, 2051−2058.
(52) Potyrailo, R. A.; Leach, A. M.; Surman, C. M. Multisize CdSe Nanocrystal/Polymer Nanocomposites for Selective Vapor Detection Identified from High-Throughput Screening Experimentation. *ACS Comb. Sci.* **2012**, *14*, 170−178.
(53) Peveler, W. J.; Roldan, A.; Hollingsworth, N.; Porter, M. J.; Parkin, I. P. Multichannel Detection and Differentiation of Explosives with a Quantum Dot Array. *ACS Nano* **2016**, *10*, 1139−1146.
(54) Bright, C. J.; Nallon, E. C.; Polcha, M. P.; Schnee, V. P. Quantum Dot and Polymer Composite Cross-Reactive Array for Chemical Vapor Detection. *Anal. Chem.* **2015**, *87*, 12270−12275.
(55) Yu, W. W.; Peng, X. Formation of High-Quality CdS and Other II-VI Semiconductor Nanocrystals in Noncoordinating Solvents: Tunable Reactivity of Monomers. *Angew. Chem., Int. Ed.* **2002**, *41*, 2368−2371.
(56) Woodruff, M. A.; Hutmacher, D. W. The Return of a Forgotten Polymer—Polycaprolactone in the 21st Century. *Prog. Polym. Sci.* **2010**, *35*, 1217−1256.
(57) Meikhail, M. S.; Abdelghany, A. M.; Awad, W. M. Role of CdSe Quantum Dots in the Structure and Antibacterial Activity of Chitosan/Poly ε-Caprolactone Thin Films. *Egypt. J. Basic Appl. Sci.* **2018**, *5*, 138−144.
(58) Pholosi, A.; Naidoo, E. B.; Ofomaja, A. E. Intraparticle Diffusion of Cr(VI) through Biomass and Magnetite Coated Biomass: A Comparative Kinetic and Diffusion Study. *S. Afr. J. Chem. Eng.* **2020**, *32*, 39−55.
(59) Abargues, R.; Rodriguez-Canto, P. J.; Albert, S.; Suarez, I.; Martínez-Pastor, J. P. Plasmonic Optical Sensors Printed from Ag−PVA Nanoinks. *J. Mater. Chem. C* **2014**, *2*, 908−915.
(60) Frasco, M.; Chaniotakis, N. Semiconductor Quantum Dots in Chemical Sensors and Biosensors. *Sensors* **2009**, *9*, 7266−7286.
(61) Choi, J.; Shin, H.; Yang, S.; Cho, M. The Influence of Nanoparticle Size on the Mechanical Properties of Polymer Nanocomposites and the Associated Interphase Region: A Multiscale Approach. *Compos. Struct.* **2015**, *119*, 365−376.

https://doi.org/10.1021/acsanm.2c00743
ACS Appl. Nano Mater. 2022, 5, 6717−6725